



## Single-grain quartz OSL dating of debris flow deposits from Men Tou Gou, south west Beijing, China

Zhao, Qiuyue ; Thomsen, Kristina Jørkov; Murray, A. S.; Wei, Mingjian ; Song, Bo

*Published in:*  
Quaternary Geochronology

*Link to article, DOI:*  
[10.1016/j.quageo.2017.06.001](https://doi.org/10.1016/j.quageo.2017.06.001)

*Publication date:*  
2017

*Document Version*  
Peer reviewed version

[Link back to DTU Orbit](#)

*Citation (APA):*  
Zhao, Q., Thomsen, K. J., Murray, A. S., Wei, M., & Song, B. (2017). Single-grain quartz OSL dating of debris flow deposits from Men Tou Gou, south west Beijing, China. *Quaternary Geochronology*, 41, 62-69.  
<https://doi.org/10.1016/j.quageo.2017.06.001>

---

### General rights

Copyright and moral rights for the publications made accessible in the public portal are retained by the authors and/or other copyright owners and it is a condition of accessing publications that users recognise and abide by the legal requirements associated with these rights.

- Users may download and print one copy of any publication from the public portal for the purpose of private study or research.
- You may not further distribute the material or use it for any profit-making activity or commercial gain
- You may freely distribute the URL identifying the publication in the public portal

If you believe that this document breaches copyright please contact us providing details, and we will remove access to the work immediately and investigate your claim.

1 **Single-grain quartz OSL dating of debris flow deposits from Men Tou Gou,**  
2 **south west Beijing, China**

3

4 Qiuyue Zhao <sup>1,2\*</sup>, Kristina Jørgkov Thomsen<sup>3</sup>, Andrew Sean Murray<sup>4</sup>, Mingjian Wei <sup>2</sup>,  
5 Bo Song<sup>5</sup>

6 <sup>1</sup>Key Laboratory of Tourism and Resources Environment in Universities of  
7 Shandong–Taishan University, 271000 Taian, China

8 <sup>2</sup>College of Resource Environment and Tourism – Capital Normal University, 100048  
9 Beijing, China

10 <sup>3</sup>Center for Nuclear Technologies, Technical University of Denmark, DTU Risø  
11 Campus, Frederiksborgvej 399, 4000 Roskilde, Denmark

12 <sup>4</sup>Nordic Laboratory for Luminescence Dating, Department of Geoscience, University  
13 of Aarhus, Risø Campus, Frederiksborgvej 399, 4000 Roskilde , Denmark

14 <sup>5</sup>Beijing Jing Yuan School, 100040 Beijing, China

15

16 \* Corresponding author: [qyzhao@cnu.edu.cn](mailto:qyzhao@cnu.edu.cn)

17

18

19 **Abstract**

20 Debris flows in the mountainous regions south west of Beijing, China occur  
21 frequently and often result in considerable mass movements with disastrous  
22 consequences for human life, infrastructure and agriculture. Obtaining chronological  
23 information on such events is important for the prediction of the return frequency of

24 these debris flows, risk assessment and climate change research. In this project, we  
25 use quartz single-grain optically stimulated luminescence (OSL) methods to  
26 determine the burial ages of five debris flow samples from the Zhai Tang region ~60  
27 km west of Beijing. OSL characteristics were found to be acceptable despite the low  
28 inherent brightness of quartz extracted from these samples. Single-grain thermal  
29 transfer was determined to be negligible and beta dose recovery experiments were  
30 satisfactory. The quartz single-grain dose distributions strongly indicate that the  
31 samples were poorly bleached prior to deposition; relative over-dispersions are larger  
32 than 60%. Minimum age modelling indicates that all five samples were deposited  
33 within the past few hundred years, indicating that catastrophic debris flows are  
34 occurring under the historically-recent land-use pattern.

35

36 Keywords

37 Quartz; Single grain OSL dating; SAR; Debris flow deposits

38

## 39 1 INTRODUCTION

40 Debris flows are frequent events in mountainous areas; in China they lead to the  
41 death of 300-600 people every year and annual losses of ~2 billion yuan  
42 (~US\$ 300M, Cui et al., 2000). Although catastrophic debris flows are an unavoidable  
43 component of the evolution of mountain landforms (Šilhán and Pánek, 2010), their  
44 impact can be reduced by quantifying risk in time and space. Fortunately, debris flow  
45 deposits provide a record of the size and frequency of debris flows, as well as of other  
46 agents of landscape evolution; they can reflect rainfall, terrain and tectonic  
47 movements (Cui et al., 1996). In the region of interest in this study, the mountainous  
48 area to the west of Beijing, a knowledge of the age of debris flow deposits, coupled  
49 with an understanding of the associated formation environment, hydrodynamic

50 conditions, and environmental evolution would help in the understanding and  
51 assessment of the modern environment and contribute to providing estimates of the  
52 likelihood of geological disasters. Unfortunately, the interpretation of the debris flow  
53 record in terms of return frequency, risk assessment, and related climate change  
54 research is limited by the availability of reliable chronological methods; organic  
55 material suitable for  $^{14}\text{C}$  dating is rare.

56 Optically Stimulated Luminescence (OSL) has the potential to determine the time  
57 elapsed since the last transport and deposition of sediment; this technique measures  
58 the time elapsed since energy trapped in crystal structures (e.g. quartz and feldspar) as  
59 a result of exposure to natural ionising radiation was last released by exposure to  
60 daylight. However, the opportunity for sufficient light exposure during debris flows is  
61 limited and thus heterogeneous resetting of the latent OSL signal is expected. Despite  
62 this, Lu et al. (2003) used fine-grain (multi-grain aliquots) OSL techniques (**infrared**  
63 **stimulated luminescence**, IRSL and **green stimulated luminescence**, GLSL) to date 9  
64 debris flow deposits samples on the Ma Lan platform (south west of Beijing) and  
65 concluded that these sediments were deposited ~7-43 ka ago, i.e. before significant  
66 anthropogenic influence and likely in a substantially different climate regime; the  
67 presence of Holocene ages indicates that at least some resetting had taken place even  
68 in such unlikely environments. Nevertheless, application of standard multi-grain OSL  
69 techniques to such deposits is likely to result in a significant over-estimation of the  
70 true burial age due to averaging effects (e.g. Olley et al., 1998). Thus, in order to  
71 identify the population of grains most likely to have been well-bleached (or well-  
72 reset) at deposition, the aliquot size must be reduced, ideally to a single grain, and  
73 minimum dose modelling applied. Wu et al. (2010) investigated single grains of  
74 quartz extracted from modern debris flow deposits in western Taiwan and found that  
75 using the lowest 5% of the single-grain doses (**Olley et al., 1998**) helped to distinguish  
76 well-bleached grains from incompletely bleached grains. Zhao et al. (2015) applied  
77 the IEU (Internal/External Consistency Criterion, Thomsen et al., 2003; 2007)

78 minimum dose model to a recent known-age (<25 years) debris flow from a small  
79 (~3.9 km<sup>2</sup>) catchment ~140 km north of Beijing and to three palaeo-deposits from a  
80 sedimentary sequence containing the evidence of multiple flow events. They obtained  
81 an age estimate for the youngest sample consistent with the known age, and minimum  
82 ages for the older palaeo-deposits suggesting that there were at least 3 major debris  
83 flows in that catchment in the last 1000 years.

84 In the densely populated and mountainous region around Beijing, debris flows  
85 have repeatedly led to mortality and significant economic loss (Xie and Cui, 1992).  
86 The aim of our study is to lay the foundation for the reconstruction of debris flow  
87 activity history in the Beijing region. Because of the likelihood of incomplete  
88 bleaching, we use quartz single-grain OSL techniques. Thermal transfer and dose  
89 recovery is first investigated and burial doses for five torrent debris flow deposits  
90 from the Men Tou Gou District (Beijing) are derived by application of the IEU  
91 minimum dose model. The regional implications of the resulting ages are then  
92 considered.

93

## 94 2 REGIONAL SETTING AND SITE DESCRIPTION

95 The study area is situated in the Zhai Tang Zhen, in the Men Tou Gou District,  
96 Beijing (39°57'28.21"N, 115°41'35.66"E); samples were taken beside the Ma Lan  
97 Gou, a southern seasonal tributary of the Qingshui River (a tributary of Yongding  
98 River) (Fig.1). The local geology is dominated by purple and grey sand shale and  
99 sandy slate, and the catchment lies in a mid-latitude eastern continental monsoon  
100 climate, with frequent rain storms between June and August; this period delivers  
101 ~75% of the annual ~677 mm precipitation. Upstream of our sampling site, the Ma  
102 Lan Gou channel is ~6 km long, with a catchment area of ~15 km<sup>2</sup> and a relative  
103 elevation of ~100 m. The steep terrain combined with intense rainstorms have led to  
104 many debris flows in the area in the historical past ( Zhao and Dong,1996; Xie et

105 al.,2001), especially the debris flows at Qing Shui and Zhai Tang in 1950, which  
106 affected 53 villages; 84 people were killed, 24 seriously injured and >80 houses were  
107 destroyed (Hong, 1995).

108 At our site, a road cuts through debris flow facies from Ma Lan Gou (Fig. 1). The  
109 exposed section sits on bedrock and is made up primarily of gravel and mixed hybrid  
110 units interleaved with sandy silt deposits. The composite section of Fig. 1c is based on  
111 four adjacent and laterally-connected exposures, individually illustrated in Fig. 1d.  
112 Some fine sand lenses are also present. The hybrid units are poorly sorted, and contain  
113 sub-rounded gravel and silty sands, with randomly oriented large clasts. These units  
114 are confidently identified as debris flow deposits.

115

## 116 3 EXPERIMENTAL DETAILS

### 117 3.1 SAMPLING

118 The freshly exposed sections were cut vertically and cleaned. OSL dating samples  
119 were collected using 5 cm diameter 25 cm long steel tubes located as shown in Fig. 1.  
120 Samples ZT-1, 3 and ZT-4 were taken from the high energy hybrid units, ZT-2 and  
121 ZT-5 were taken from the interleaved lower energy sandy silts (see also Table 1). We  
122 interpret samples ZT-1, 2, 3 to have been deposited during the early stages of debris  
123 flow, and samples ZT-4,5 to have been deposited as the mass movement ceased, or  
124 afterwards. Aluminium foil was used to pack and wrap the two ends of the tube to  
125 prevent sample mixing during transport. Samples preparation was carried out under  
126 subdued red light and material from the two ends of the sampling tubes was removed  
127 for dose rate and water content measurement; sediment from the middle part of the  
128 sampling tubes was used for  $D_e$  estimation (see below).

129

## 130 3.2 SAMPLE PREPARATION

131 The material collected for OSL measurements was firstly wet-sieved to give the  
132 180-250  $\mu\text{m}$  grain size fraction. The grains were then treated with 10% hydrochloric  
133 acid (HCl) and 10% hydrogen peroxide ( $\text{H}_2\text{O}_2$ ) to remove carbonates and organic  
134 matter. Density separation used sodium polytungstate heavy liquid of density 2.58 and  
135  $2.70 \text{ g cm}^{-3}$  to separate a quartz-rich fraction. To remove the alpha irradiated skin and  
136 any remaining feldspar contamination, the quartz fractions were then etched with 40%  
137 hydrofluoric acid (HF) for 60 min, and washed in 10% HCl for 40 min to remove any  
138 fluoride precipitates. Any remaining feldspar contamination in quartz was checked by  
139 infrared (IR) stimulation to confirm that no samples gave a significant IR signal  
140 (compared to blue OSL). All samples were re-sieved after chemical treatment to the  
141 size fraction 180-250  $\mu\text{m}$ .

142

## 143 3.3 INSTRUMENTATION AND ANALYSIS

144 All OSL measurements were made using Risø TL/OSL DA-20 readers (Bøtter-  
145 Jensen et al., 2003; 2010). Single-grain OSL measurements were made using the Risø  
146 single-grain attachment. Luminescence signals were detected using a combination of  
147 a bialkali EMI 9235QB photomultiplier tube and a 7.5 mm Hoya U-340 filter. Single  
148 grain OSL measurements made use of a 10 mW green Nd:YVO<sub>4</sub> solid diode-pumped  
149 laser emitting at 532 nm and providing a power density of  $\sim 50 \text{ W cm}^{-2}$  (Duller et al.,  
150 1999). Arrays of blue (470 nm) LEDs providing a power density of  $\sim 40 \text{ mW cm}^{-2}$  at  
151 the sample position were used in multi-grain measurements. Green laser stimulation  
152 was for 0.9 s at 125 °C whereas blue LED stimulation was for 40 s at 125 °C.

153 For single-grain measurements individual quartz grains (180-250  $\mu\text{m}$ ) were  
154 loaded into aluminium single-grain measurement discs each containing a  $10 \times 10$   
155 matrix of grain holes (depth and diameter of 300  $\mu\text{m}$ ). For multi-grain measurements,

156 quartz grains were mounted in a monolayer on 9.7 mm stainless steel discs using  
157 silicone oil. Each multi-grain aliquot contained about 150 grains.

158 Calibrated  $^{90}\text{Sr}/^{90}\text{Y}$  beta sources ( $\sim 0.1 \text{ Gy}\cdot\text{s}^{-1}$ ) fitted on the Risø TL/OSL-DA-20  
159 readers were used for laboratory irradiations. The dose rates delivered by these beta  
160 sources varied by  $<5\%$  (standard deviation) across the sample area. Correcting for  
161 spatial non-uniformity of the sources (Lapp et al., 2012) did not result in significant  
162 changes to measured dose or over-dispersion (OD).

163 The single-aliquot regenerative dose (SAR) procedure (Murray and Wintle, 2000,  
164 2003; Wintle and Murray, 2006) was used for dose estimation. A preheat of  $200^\circ\text{C}$   
165 for 10 s, a cut heat of  $180^\circ\text{C}$ , a heating rate of  $5^\circ\text{C s}^{-1}$ , and a 4.5 Gy test dose were  
166 used in all dose measurements. The dose response curves consisted of a minimum of  
167 three regeneration doses, a zero dose point (i.e. a measurement of recuperation) and a  
168 repeat (recycling) point. In addition, each aliquot was checked for feldspar  
169 contamination by the measurement of the IR depletion ratio (Duller, 2003). For  
170 single-grain measurements, the largest regeneration dose given was 160 Gy; all  
171 single-grain doses larger than 160 Gy are derived using extrapolation and these dose  
172 estimates are thus likely to be less reliable.

173 Multi-grain signals were derived from the summation of the initial 0.64 s of  
174 stimulation. The immediately following 0.64 s of stimulation was used for  
175 background subtraction. Single-grain signals were derived from the summation of the  
176 first 0.06 s of the stimulation curves and the last 0.16 s of stimulation was used for  
177 background subtraction. Sensitivity-corrected OSL dose-response curves were fitted  
178 using a single saturation exponential function, passing through the origin.

179 Only  $D_e$  estimates with a relative uncertainty of the natural test dose signal less  
180 than 30% were accepted ( $s_{Tn} < 30\%$ ). In addition, dose estimates were accepted only if  
181 (i) recycling and IR depletion ratios lay between 0.8 and 1.2 and (ii) sensitivity  
182 corrected recuperation signals were consistent with 0 at two standard deviations. No



183 dose estimates could be derived for ~46% of the otherwise accepted grains, because  
184 the sensitivity corrected natural signal was in saturation on the laboratory dose  
185 response curve.

186 These criteria led to the rejection of 99% of the measured single grains. In  
187 addition, 54% of the multi-grain aliquots gave sensitivity-corrected natural signals  
188 that lay at or above saturation of the laboratory dose-response curve (out of a total of  
189 54 aliquots of sample ZT-1, -2, -4.)

#### 190 4 DOSE RATES

191 By their nature, the deposits are very heterogeneous, but every effort was made  
192 to take OSL samples at least 10 cm from the nearest large clast, to minimise the risk  
193 of significant perturbation of the gamma dose rate. Potentially light-exposed material  
194 (~80 g) taken from the ends of the sample tube was ground and homogenized, cast in  
195 wax and stored for more than 21 days to ensure equilibrium between  $^{226}\text{Ra}$  and  $^{222}\text{Rn}$ .  
196 The radionuclide concentrations were then measured using calibrated high resolution  
197 gamma spectrometers (Murray et al., 1987). Dose rates (Table 1) derived from the  
198 radionuclide concentrations of  $^{238}\text{U}$ ,  $^{232}\text{Th}$  and  $^{40}\text{K}$  were derived using the conversion  
199 factors provided by Guérin et al. (2011), and the cosmic ray contribution is based on  
200 Prescott and Hutton (1994). The water content is the average of observed and  
201 saturated water content.

#### 202 5 LUMINESCENCE CHARACTERISTICS

203 Multi-grain aliquots (~150 grains each) were first measured to assess the  
204 suitability of these samples for OSL dating. Fig. 2 shows a normalised OSL decay  
205 curve from a multi-grain aliquot from sample ZT-2 (open triangles) and from  
206 calibration quartz (filled circles). The latter is known to be fast component dominated  
207 (Hansen et al., 2015), and the comparison demonstrates that the OSL signal from ZT-  
208 2 is also fast-component dominated. The inset in Fig. 2 shows a typical dose response

209 curve from multi-grain aliquots, fitted with a single saturating exponential function  
210 passing through the origin.

## 211 5.1 THERMAL TRANSFER AND DOSE RECOVERY

212 Single-grain thermal transfer was measured for sample ZT-2 using a preheat of  
213 200 °C for 10 s and a cutheat of 180 °C, by initially bleaching the sample using the  
214 blue LEDs twice for 100 s with an intervening pause of 10,000 s. The resulting dose  
215 distribution (Fig. 3a) has an arithmetic average dose of  $340 \pm 190$  mGy ( $n=20$ ). The  
216 corresponding  $CAM_{UL}$  (Arnold et al., 2009) dose is  $180 \pm 160$  mGy ( $CAM_{UL}$  is used  
217 because of the presence of non-positive dose estimates). We then performed three  
218 beta dose recovery experiments using sample ZT-1, ZT-3 and ZT-4, respectively (Fig.  
219 3b,c, and d). The grains were loaded into the single-grain discs and bleached as before  
220 prior to being given beta doses of 0.9 Gy (ZT-1,  $N=3000$ , Fig. 3c), 3 Gy (ZT-3,  
221  $N=3300$ , Fig. 3b) and 6 Gy (ZT-4,  $N=2300$ , Fig. 3d), respectively. The resulting dose  
222 recovery ratios are  $0.92 \pm 0.16$  ( $n=23$ ,  $OD=51 \pm 22\%$ ,  $CAM_{UL}$ ),  $0.99 \pm 0.09$  ( $n=24$ ,  
223  $OD=33 \pm 7\%$ ,  $CAM$ ) and  $0.96 \pm 0.05$  ( $n=28$ ,  $OD=17 \pm 7\%$ ,  $CAM$ ), respectively. We  
224 deduce that our chosen SAR protocol is able to measure a laboratory dose given to  
225 these samples before any thermal treatment with sufficient accuracy.

226 If we do not make use of the standard rejection criteria given in section 3.3  
227 (except for  $s_{Tn} < 30\%$ ) the corresponding dose recovery ratios are  $1.04 \pm 0.14$  ( $n=27$ ,  
228  $OD=50 \pm 16\%$ ),  $1.02 \pm 0.07$  ( $n=40$ ,  $OD=33 \pm 5\%$ ) and  $0.96 \pm 0.05$  ( $n=31$ ,  $OD=16 \pm 7\%$ ),  
229 respectively. We conclude that applying the standard rejection criteria does not  
230 significantly change the measured dose or the OD, but these criteria do reduce the  
231 accepted grain population by  $\sim 20\%$ , on average.

232

## 233 5.2 D<sub>E</sub> DISTRIBUTION AND ANALYSIS

234 A total of >29,000 individual grains (at least 4,800 for each sample, see Table 2)  
235 were measured for the five natural samples. After application of the standard rejection  
236 criteria, between 0.8 and 1.0% of the grains gave results accepted into the dose  
237 distribution and the majority of these grains were only weakly luminescent; the  
238 median of the intensity of the test dose signal of the accepted grains was 8.3 Gy<sup>-1</sup>  
239 (summed over the initial 60 ms of stimulation; 273 grains, 5 samples).

240 The five natural single-grain dose distributions are shown as scatter plots in Fig.  
241 4, where the OSL signals from the natural test dose are plotted against the equivalent  
242 dose. The doses range broadly between 0 and 300 Gy, but note that dose  
243 estimates larger than 160 Gy (see section 3.3) are derived by extrapolation and are not  
244 necessarily accurate. All dose distributions are significantly positively skewed with  
245 OD values ranging between 65±10 and 138±29% and a 'leading edge' at low D<sub>e</sub>  
246 values. This indicates that these samples may not have been completely bleached  
247 before deposition and thus that multi-grain analysis may significantly over-estimate  
248 the time of the last deposition.

249 To derive realistic deposition ages, it is very likely that minimum dose modelling  
250 must be applied to the natural single-grain dose distributions in order to identify the  
251 grains most likely to have been well-bleached at deposition. Here we apply the IEU  
252 minimum dose model (Thomsen et al., 2007; Smedley 2015) making use of the results  
253 from the thermal transfer and beta dose recovery experiments described in section 5.1  
254 as input parameters, i.e. values of *a* and *b* of 0.14±0.09 and 0.35±0.17 Gy,  
255 respectively. The grains identified as well-bleached using this approach are shown in  
256 Fig. 4 as filled symbols and the derived minimum burial doses D<sub>b</sub> are given in Table  
257 2. The relative number of grains identified as well-bleached range between 13 and  
258 50%. The sample expected to be youngest (ZT- 5) has the highest proportion of well-  
259 bleached grains.

260 In the above analysis, we have only included individual dose estimates which pass  
261 the standard rejection criteria given in section 3.3, although the dose recovery  
262 experiments showed that applying these criteria led to the rejection of ~20% of the  
263 grain population without any significant change to measured dose or over-dispersion.  
264 If we now consider dose estimates based on all grains with  $s_{Tn} < 30\%$  (i.e. not using  
265 other standard rejection criteria), then the average ratio of  $D_b$  calculated using grains  
266 passing all the rejection criteria to grains only passing  $s_{Tn} < 30\%$  is  $0.99 \pm 0.04$  ( $n=5$   
267 samples), but the average relative uncertainty on individual dose estimates is ~30%  
268 larger if all standard rejection criteria are used. Thus, using the all the standard  
269 rejection criteria has no impact on the absolute minimum doses determined, but the  
270 precision of the minimum dose estimates is decreased. Similar observations have been  
271 made by Thomsen et al., (2012), Geach et al. (2015), Guérin et al. (2015b), Hansen et  
272 al. (2015), Kristensen et al. (2015), Zhao et al., (2015); Guérin et al. (2016),  
273 Thomsen et al., (2016).

274 Using minimum dose modelling relying on individual uncertainties to derive  
275 minimum dose is usually very dependent on the assigned uncertainties (e.g. Thomsen  
276 et al., 2007; Medialdea et al., 2014). In the above, we implicitly assumed that the  
277 dispersion observed in the beta dose recovery experiments is similar to the dispersion  
278 to be expected in a naturally well-bleached dose distribution of the same material.  
279 However, this is unlikely to be an accurate approach in samples that, for instance,  
280 were exposed to a heterogeneous environmental beta dose (e.g. Thomsen et al., 2007,  
281 Guérin et al., 2015). To investigate how sensitive our minimum dose estimates are to  
282 the size of the assigned additional uncertainty the additional uncertainty input  
283 parameter ( $a$ ) was varied between 10 and 40%, i.e. varied over the range of over-  
284 dispersions commonly reported for well-bleached dose distributions (e.g. Arnold and  
285 Roberts, 2009). Fig. 5 shows how the estimated burial dose  $D_b$  (normalized to the  
286 value derived using  $a = 14\%$ , as derived from the beta dose recovery experiments)  
287 varies as a function of  $a$ . For a given sample, all estimates of  $D_b$  are consistent with

288 each other although there is, as expected, a systematic increase in  $D_b$  with  $a$ . The  
289 average ratio of  $D_b$  calculated using an  $a$  value of 40% to that calculated using a value  
290 of 14% is  $1.44 \pm 0.08$  ( $n=5$  samples).

291

### 292 5.3 SYNTHETIC ALIQUOT RESULTS

293 Although we focus on measurement of single-grains in this study, it is interesting  
294 to examine the doses that would have been measured using small multi-grain aliquots.  
295 Given the inherently low OSL sensitivity of these samples (few grains giving  
296 detectable OSL signals and most grains that are detectable have dim OSL signals),  
297 measurements of small multi-grain aliquots, each containing  $\sim 100$  grains, might be  
298 expected to behave as single grain measurements, and so give dose distributions  
299 from which one could derive accurate deposition doses. As there was insufficient  
300 sample to undertake both single-grain and multi-grain measurements, we here  
301 examine the difference between these two approaches by combining the OSL signals  
302 from individual single-grain discs (each containing 100 single grains) to generate  
303 “synthetic” multi-grain aliquots. The synthetic multi-grain  $CAM_{UL}$  doses are given in  
304 Table 2; these range between 29 and 62 Gy and are very similar to the corresponding  
305  $CAM_{UL}$  doses for the single-grain measurements (with the exception of sample ZT-2).  
306 However, none of these synthetic aliquots give doses smaller than 2 Gy and thus  
307 minimum dose modelling would significantly overestimate that of single-grain  
308 minimum dose modelling (see Table 2). Thus, despite of the low OSL sensitivity of  
309 these samples, multi-grain measurements ( $\sim 100$  grains per aliquot) are likely to  
310 produce significant overestimates of the burial age compared to those provided by  
311 true single-grain measurements.

312

314 The resulting single-grain OSL ages are given in Table 2. The five weighted  
315 average ( $CAM_{UL}$ ) ages range from  $7 \pm 1$  to  $22 \pm 4$  ka, similar to that from the synthetic  
316 multi-grain ages ( $13 \pm 3$  to  $24 \pm 4$  ka) and to fine-grain IRSL and GLSL results reported  
317 by Lu et al., 2003. However, these average ages are affected by incomplete bleaching  
318 and thus significantly overestimate the burial age.

319 It is likely that minimum dose modelling of single-grain dose distributions  
320 provides a more accurate estimate of the burial dose. However, the calculated  
321 minimum doses from minimum dose modelling are dependent on the size of the  
322 assigned uncertainties (see Fig. 5). In the literature, it has often been argued that a  
323 “typical” over-dispersion for well-bleached samples is 15-20% (e.g. Arnold et al.,  
324 2008; Demuro et al., 2008; Turney et al., 2008), i.e. an additional uncertainty of 15-  
325 20% should be added to estimates of uncertainty based on intrinsic sources of  
326 variability (e.g. Poisson statistics, curve fitting errors etc.). Others (e.g. Thomsen et  
327 al., 2007; Medialdea et al., 2014; Sim et al., 2014) have argued that it would be more  
328 appropriate to use an additional uncertainty based on the over-dispersion determined  
329 in laboratory dose recovery experiments (preferably irradiated using a gamma  
330 source), although the latter approach presumably underestimates for samples exposed  
331 to significant dose rate heterogeneity during burial. However, Guérin et al. (2015)  
332 showed beta dose heterogeneity arising from non-uniform distribution of potassium in  
333 the sediment is of concern “*when the average grain size is in the sand and gravel*  
334 *range (rather than silt or clay), the potassium content is low (<1%), and the total*  
335 *dose rate is small (<1 Gy ka<sup>-1</sup>)”*. Thus, at this stage, it is less likely that our samples  
336 are significantly affected by beta dose rate heterogeneity. In any case, based on the  
337 beta dose-recovery experiments, the minimum uncertainty with which an individual  
338 dose estimate can be known is  $14 \pm 9\%$ , although we acknowledge that this over-  
339 dispersion may be underestimated. Nonetheless, this minimum additional uncertainty

340 must be added (in quadrature) to the uncertainties assigned to individual dose  
341 estimates based on Poisson statistics and dose response curve fitting errors, if a true  
342 minimum estimate of uncertainty on individual single grain dose estimates is to be  
343 used in later analysis.

344 The minimum single-grain (IEU) ages (using an additional uncertainty of 14%,  
345 see Table 2) are all consistent with an average age of  $320 \pm 25$  y and there appears to  
346 be no stratigraphic relationship between ages of the samples. If an additional  
347 uncertainty of 40% is assumed, all IEU ages are consistent with an average age of  
348  $470 \pm 50$  y. Thus, we conclude that these debris flow samples were all deposited in a  
349 short span of time (<100 years) within the last 500 years.

350 Giving the influence of insufficiently bleached grains on the OSL signal in  
351 these debris flows, the single-grain ages are much smaller than those from multi-grain  
352 measurements (Lu et al., 2003) and simulated multi-grain data. These debris flows  
353 were apparently deposited around 300-500 y ago, during the Little Ice Age in China  
354 (Zhu et al., 1973), which may indicate an association of debris flows in this area with  
355 cold periods or perhaps unstable periods of cold and warm fluctuation.

356 However, the importance of the anthropogenic-induced deterioration of the  
357 regional natural environment must also be considered. According to historical  
358 documents (Hou et al., 1985), significant deforestation in Xishan (Zhai Tang is in the  
359 Xishan mountain basin) in this period was associated with the Yuan Dynasty (AD  
360 1271–1368) construction of a new capital in Beijing. Initially, a large amount of  
361 building construction material, and charcoal for cooking and heating, was taken from  
362 Xishan. Subsequently during the Ming Dynasty (AD 1368–1644), Beijing's  
363 increasing demand for raw materials continued the unsustainable exploitation of the  
364 vegetation of the Xishan region. This was exacerbated by the increase in local  
365 population, which more than doubled from 300,000 to 670,000; this must also have  
366 increased pressure on agriculture. The resulting landscape degradation presumably led

367 to increased runoff; certainly there were frequent floods from ~650 to ~360 years ago  
368 in the Lugu (now Yongding) River, into which the Ma Lan Gou feeds (Hou et al.,  
369 1985). We deduce that the Zhai Tang debris flow deposits may represent geological  
370 evidence for the prolonged destruction of forest resources after the establishment of  
371 Yuan Dynasty capital in Beijing.

372

## 373 7 CONCLUSION

374 OSL dating of these debris flow deposits has proved challenging because of  
375 significant incomplete bleaching and the inherently low luminescence sensitivity of  
376 individual grains. Equivalent dose distributions are significantly positively skewed,  
377 with clearly identifiable leading edges at low doses. Using doses derived from  
378 simulated multi-grain data (synthetic aliquots) the ages of these deposits range  
379 between  $13 \pm 3$  and  $24 \pm 4$  ka, very similar to previously published fine-grain ages (Lu  
380 et al., 2003) and average single-grain ages. However, using single-grain dose  
381 distributions in combination with minimum dose modelling, the relative number of  
382 grains identified to be well-bleached range between 13 and 50%, strongly suggesting  
383 that multi-grain OSL techniques greatly overestimated the burial ages for these  
384 samples. We conclude that these debris flow samples were probably all deposited in a  
385 short span of time (<100 years) within the last 500 years, and tentatively associate  
386 these sediments with the historically-recorded catchment exploitation. Our results are  
387 of direct relevance to the assessment of mass movement hazard in the Men Tou Gou  
388 District, and we conclude that there is no evidence to suggest that the current risk of  
389 further debris flows has been mitigated.

390

391

392



393 ACKNOWLEDGEMENTS

394 This research was supported by the National Natural Science Foundation of China  
395 (NSFC, Grant No. 40871017, 41602353, 41471007 and 41301006 ) and Social Science  
396 Foundation of China (Grant No. 15CJY073). We are indebted to Yanyan Tian, Rui  
397 Zhou, Hongyi Chen, Yugeng Liu and Jian Pan for assistance during field work. We  
398 thank Shuzhen Peng and Min Ding for providing valuable comments on this  
399 manuscript.

400

401 REFERENCES

402

403 Arnold, L.J., Roberts, R.G., Galbraith, R.F., Delong, S.B., 2009. A revised burial dose  
404 estimation procedure for optical dating of young and modern-age sediments. *Quat.*  
405 *Geochronol.* 4, 306-325.

406 Bøtter-Jensen, L., Andersen, C.E., Duller, G.A.T., Murray, A.S., 2003. Developments  
407 in radiation, stimulation and observation facilities in luminescence measurements.  
408 *Radiat. Meas.* 37, 535-541.

409 Bøtter-Jensen, L., Thomsen, K.J., Jain, M., 2010. Review of optically stimulated  
410 luminescence (OSL) instrumental developments for retrospective dosimetry.  
411 *Radiat. Meas.* 45, 253-257.

412 Cui, P., Liu, S.J., Tan, W.P., 2000. Progress of debris flow forecast in China. *Journal*  
413 *of Natural Disasters.* 9 (2): 10-15 (in Chinese).

414 Cui, Z.J., 1996. Debris flow deposit and environment. China Ocean Press, Beijing, 1-  
415 188 (in Chinese).

416 Duller, G.A.T., Bøtter-Jensen, L., Murray, A.S., Truscott, A.J., 1999. Single grain  
417 laser luminescence (SGLL) measurements using a novel automated reader. *Nucl.*  
418 *Instrum. Methods Phys. Res. B: Beam Interact. Mater. Atoms.* 155(4), 506-514.

419 Duller, G.A.T., 2003. Distinguishing quartz and feldspar in single grain luminescence  
420 measurements. *Radiat. Meas.* 37, 161-165.

421 Fuchs, M., Straub, J., Zöller, L., 2005. Residual luminescence signals of recent river  
422 flood sediments: a comparison between quartz and feldspar of fine- and coarse-  
423 grain sediments. *Ancient TL.* 23(1), 25-30.

424 Geach, M. R., Thomsen, K. J., Buylaert, J.-P., Murray, A. S., Mather, A. E., Telfer,  
425 M. W., 2015. Single-grain and multi-grain OSL dating of river terrace sediments  
426 in the Tabernas Basin, SE Spain. *Quat. Geochron.* 2015, 213-218.

427 Godfrey-Smith, D.I., Huntley, D.J., Chen, W.H., 1988. Optical dating studies of  
428 quartz and feldspar sediment extracts. *Quat. Sci. Rev.* 7(3~4), 373-380.

429 Guérin, G., Mercier, N., Adamic, G., 2011. Dose-rate conversion factors: update.  
430 *Ancient TL*, 29, 5-8.

431 Guérin, G., Jain, M., Thomsen, K., Murray, A., Mercier, N., 2015. Modelling dose  
432 rate to single grains of quartz in well-sorted sand samples: the dispersion arising  
433 from the presence of potassium feldspars and implications for single grain OSL  
434 dating. *Quaternary Geochronology*, 27, 52-65.

435 Guérin, G., Combès, B., Lahaye, C., Thomsen, K.J., Tribolo, C., Urbanova, P., Guibert,  
436 P., Mercier, N., Valladas, H., 2015a. Testing the accuracy of a Bayesian central-  
437 dose model for single-grain OSL, using known-age samples. *Radiation*  
438 *Measurements* 81, 62-70

439 Guérin, G., Frouin, M., Talamo, S., Aldeias, V., Bruxelles, L., Chiotti, L., Dibble, H.L.,  
440 Goldberg, P., Hublin, J.-J., Jain, M., Lahaye, C., Madelaine, S., Maureille, B.,  
441 McPherron, S.P., Mercier, N., Murray, A.S., Sandgathe, D., Steele, T.E., Thomsen,  
442 K.J., Turq, A., 2015b. A multi-method luminescence dating of the Palaeolithic  
443 sequence of La Ferrassie based on new excavations adjacent to the La Ferrassie 1  
444 and 2 Skeletons. *J. Archaeol. Sci.* 58, 147-166.

445 Guérin, G., Frouin, M., Tuquoi, J.; Thomsen, K.J., Goldberg, P., Aldeias, V., Lahaye,  
446 Ch., Mercier, N., Guibert P., Jain, M., Sandgathe, D., McPherron, S.P., Turq, A.,  
447 Dibble, H.L., 2016. The complementarity of luminescence dating methods  
448 illustrated on the Mousterian sequence of the Roc de Marsal: A series of reindeer-  
449 dominated, Quina Mousterian layers dated to MIS 3. *Quaternary International*, in  
450 press.

451 Hansen, L., Funder, F., Murray, A.S., Mejdahl, V., 1999. Luminescence dating of the  
452 last Weichselian Glacier advance in East Greenland. *Quat. Sci. Rev.* 18(2), 179-  
453 190.

454 Hansen, V., Murray, A.S., Buylaert, J-P., Yeo, E-Y., Thomsen, K.J. 2015. A new  
455 irradiated quartz for beta source calibration. *Radiation Measurements* 81, 123-  
456 127.

457 Hong, C.S., 1995. Occurrence and Countermeasures of debris flow in Beijing. Beijing  
458 water conservancy. 4: 7-10.

459 Hou, R.Z., 1985. The Historical Atlas of Beijing. Beijing Press. pp. 127(in Chinese).

460 Jain, M., Murray, A.S., Bøtter-Jensen, L., 2003. Characterisation of blue-light  
461 stimulated luminescence components in different quartz samples: implications for  
462 dose measurement. *Radiat. Meas.* 37(4-5), 441-449.

463 Kristensen, J.A., Thomsen, K.J., Murray, A.S., Buylaert, J.P., Jain, M., Breuning-  
464 Madsen, H., 2015. Quantification of termite bioturbation in a savannah ecosystem:  
465 application of OSL dating. *Quat. Geochronol.* 30, 334-341.

466 Lapp, T., Jain, M., Thomsen, K.J., Murray, A.S., Buylaert, J.P., 2012. New  
467 luminescence measurement facilities in retrospective dosimetry. *Radiat. Meas.* 47,  
468 803-808. 611-620.

469 Lu, Y.C., Wei, L.Y., Yin, J.H., Yin, G.M., Zhao, H., 2003. Dates and environments of  
470 the Malan gravel formation as the torrent debris deposits along Qingshui River in  
471 western hills, Beijing. *Quaternary Sciences.* 23(6), 611-620.

472 Medialdea, A., Thomsen, K.J., Murray, A.S., Benito, G., 2014. Reliability of  
473 equivalent-dose determination and age-models in the OSL dating of historical and  
474 modern palaeoflood sediments. *Quat. Geochronol.* 22, 11-24.

475 Mejdahl, V., 1987. Internal radioactivity in quartz and feldspar grains. *Ancient TL.* 5,

476 10-17.

477 Murray, A.S., Marten, R., Johnston, A., Martin, P., 1987. Analysis for naturally  
478 occurring radionuclides at environmental concentrations by gamma spectrometry. J.  
479 Radioanal. Nucl. Chem. 115(2), 263-288.

480 Murray, A.S., Wintle, A.G., 2000. Luminescence dating of quartz using an improved  
481 single-aliquot regenerative-dose protocol. Radiat. Meas. 32, 57-73.

482 Murray, A.S., Wintle, A.G., 2003. The single aliquot regenerative dose protocol:  
483 potential for improvements in reliability. Radiat. Meas. 47(9), 688-695.

484 Murray, A.S., Thomsen, K.J., Masuda, N., Buylaert, J.P., Jain, M., 2012. Identifying  
485 well-bleached quartz using the different bleaching rates of quartz and feldspar  
486 luminescence signals. Radiat. Meas. 47(9), 688-695.

487 Olley J.M., Caitcheon G.C., and Murray A.S., 1998. The distribution of apparent dose  
488 as determined by optically stimulated luminescence in small aliquots of fluvial  
489 quartz: implications for dating young sediments. Quaternary Science Reviews  
490 (Quaternary Geochronology) 17, 1033-1040.

491 Prescott, J.R., Hutton, J.T., 1994. Cosmic ray contributions to dose rates for  
492 luminescence and ESR: large depths and long-term time variations. Radiat. Meas.  
493 23, 497-500.

494 Šilhán, K., Pánek, T., 2010. Fossil and recent debris flows in medium-high mountains  
495 (Moravskoslezská Beskydy Mts, Czech Republic). Geomorphology. 124, 238-  
496 249.

497 Sim, A.K., Thomsen, K.J., Murray, A.S., Jacobsen, G., Drysdale, R., Erskine, W.,  
498 2014. Dating recent floodplain sediments in the Hawkesbury-Nepean river system  
499 using single grain quartz OSL. Boreas, 43(1), 1-21.

500 Thomsen, K. J., Murray, A. S., Bøtter-Jensen, L., Jungner, H., 2003. Variation with  
501 depth of dose distributions in single grains of quartz extracted from an irradiated  
502 concrete block. *Radiation Measurements*, 37 (4-5), 315-321.

503 Thomsen, K.J., Murray, A.S., Bøtter-Jensen, L., Kinahan, J., 2007. Determination of  
504 burial dose in incompletely bleached fluvial samples using single grains of quartz.  
505 *Radiat. Meas.* 42 (3), 370-379.

506 Thomsen K.J., Murray A., Jain M., 2012. The dose dependency of the over-dispersion  
507 of quartz OSL single grain dose distributions. *Radiation Measurements* 47, 732-  
508 739.

509 Thomsen, K. J., Murray, A. S., Buylaert, J. P., Jain, M., Hansen, J. H., Aubry, T.,  
510 2016. Testing single-grain quartz OSL methods using sediment samples with  
511 independent age control from the Bordes-Fitte rockshelter (Roches d'Abilly site,  
512 central France). *Quat. Geochron.* 31, 77-96.

513 Wintle, A.G., 1973. Anomalous fading of thermoluminescence in mineral samples.  
514 *Nature.* 245, 143-144.

515 Wintle, A.G., Murray, A.S., 2006. A review of quartz optically stimulated  
516 luminescence characteristics and their relevance in single-aliquot regeneration  
517 dating protocols. *Radiat. Meas.* 41, 369-391.

518 Wu, T. S., Jaiswal, M.K., Lin, Y.N., Chen, Y.W., Chen, Y.G., 2010. Residual  
519 luminescence in modern debris flow deposits from western Taiwan: A single grain  
520 approach. *J Asian Earth Sci.* 38, 274-282.

521 Xie, H., Zhong, D.L., Jin, H.C., 2001. Debris flow and landslide disasters control in  
522 Mountain area of Beijing Cicy. *Bulletin of Soil and Water Conservation.*  
523 21(3):37-45(In Chinese).

524 Xie, Y.Y., Cui, Z.J., 1992. Prevention and forecast of debris flow in Beijing mountain  
525 area. *Guizhou Science*. 3, 132(In Chinese).

526 Zhao, B., Dong, G.Z., 1996. Mud-rock flows and its dangerous prediction in the  
527 drainage area of the Qingshui River, Xishan Mt., Beijing. *Geology of Beijing*. 3:  
528 1-14(In Chinese).

529 Zhao, Q., Thomsen, K.J., Murray, A.S., Wei, M., Pan, B., Song, B., Zhou, R., Chen,  
530 S., Zhao, X., Chen, H., 2015. Testing the use of OSL from quartz grains for dating  
531 debris flows in Miyun, northeast Beijing, China. *Quaternary Geochronology*. 30,  
532 320-327.

533 Zhu, K.Z., 1873. A preliminary study on climate change in China in recent 5000  
534 years. *Science in China (B)*. 3(02): 115-120(In Chinese).

535

536 **Figure captions**

537

538

539 Figure 1: Location of the study site. (a) **Regional map of study area.** (b) Composite  
540 section based on the four adjacent sampled sections illustrated in (c).

541

542 Figure 2: Multi-grain (~150 grains) quartz OSL characteristic for sample ZT-2  
543 (preheat 200 °C for 10 s, cutheat 180 °C). (a) Normalised luminescence  
544 signals from calibration quartz (filled circle) and ZT-2 (open triangles).  
545 (b) Representative dose response curve for sample ZT-2 showing  
546 recycling and recuperation (open square and diamond symbols,  
547 respectively) and the interpolation of the sensitivity-corrected natural  
548 signal (filled circle) onto the dose response curve.

549

550 Figure 3: (a) Single-grain thermal transfer dose distribution for sample ZT-2. (b)-  
551 (d) Single-grain beta dose recovery distribution for samples ZT-3 (given  
552 dose of 3 Gy), ZT-1 (0.9 Gy) and ZT-4 (6 Gy), respectively.

553

554 Figure 4: Single-grain dose distributions (open symbols) for the five natural  
555 samples. The natural test dose response (4.5 Gy) is shown as a function  
556 of estimated dose. Filled symbols represents the grains identified by the  
557 IEU model to be well-bleached using a dispersion value  $a$  of 0.14. The  
558 insets show the same data for doses less than 19 Gy.

559

560 Figure 5: Variation of the estimated burial dose  $D_b$  (normalized to the value using  
561  $a = 14\%$ ) as a function of the additional uncertainty input parameter  $a$ .

562

563



Sample code	Depth (m)	w.c. (%)	Radionuclide (Bq/ kg)				Dose rate (Gy/ka)		
			U-238	Ra-226	Th-232	K-40	dry $\beta$	dry $\gamma$	Total
ZT-1	10	22	37 $\pm$ 15	27 $\pm$ 1.1	38.3 $\pm$ 1.2	527 $\pm$ 18	1.77 $\pm$ 0.07	1.06 $\pm$ 0.03	2.35 $\pm$ 0.14
ZT-2	9	10	27 $\pm$ 12	27 $\pm$ 0.9	41.1 $\pm$ 0.9	595 $\pm$ 18	1.91 $\pm$ 0.06	1.14 $\pm$ 0.03	2.61 $\pm$ 0.16
ZT-3	8	14	26 $\pm$ 15	31 $\pm$ 1.2	44.3 $\pm$ 1.2	574 $\pm$ 22	1.89 $\pm$ 0.08	1.19 $\pm$ 0.04	2.77 $\pm$ 0.18
ZT-4	3	26	33 $\pm$ 10	27 $\pm$ 0.8	42.3 $\pm$ 0.8	551 $\pm$ 13	1.84 $\pm$ 0.05	1.13 $\pm$ 0.03	2.22 $\pm$ 0.11
ZT-5	0.4	16	30 $\pm$ 17	27 $\pm$ 1.3	35.1 $\pm$ 1.4	466 $\pm$ 19	1.58 $\pm$ 0.08	0.97 $\pm$ 0.04	2.13 $\pm$ 0.12

Table1 Summary of depth, water content (w.c.), radionuclide concentrations and quartz dose rates for the four debris flow samples. Water content is taken as midway between observed and saturated water content. An internal quartz dose rate of  $0.06 \pm 0.03$  mGy a<sup>-1</sup> has been assumed (Mejdahl, 1987). Total dose rate include cosmic rays and effect of water content.

Sample code	MG			SG							
	n <sub>1</sub>	CAM <sub>UL</sub> (Gy)	N	n <sub>2</sub>	CAM <sub>UL</sub> (Gy)	OD <sub>UL</sub> (%)	n <sub>w.b.14%</sub>	IEU D <sub>b</sub> (Gy)	Age <sub>14%</sub> (a)	n <sub>w.b.40%</sub>	Age <sub>40%</sub> (a)
ZT-1	17	41 ± 7	6500	63	37 ± 5	90 ± 15	9	0.8 ± 0.3	340 ± 140	9	490 ± 160
ZT-2	15	62 ± 8	4800	46	33 ± 6	98 ± 19	10	0.8 ± 0.3	320 ± 110	12	430 ± 150
ZT-3	17	52 ± 8	5800	47	60 ± 9	102 ± 18	6	0.9 ± 0.3	310 ± 120	7	620 ± 210
ZT-4	30	55 ± 5	6300	61	48 ± 5	65 ± 10	8	0.5 ± 0.3	240 ± 130	9	320 ± 140
ZT-5	20	29 ± 5	6000	56	15 ± 3	138 ± 29	28	0.8 ± 0.2	390 ± 70	36	510 ± 90

Table 2. Summary of synthetic multi-grain (MG) and single-grain (SG) results. 'MG' is simulated multi-grain measurements (i.e. synthetic aliquots, see text for details), 'SG' is single-grain measurements, 'n<sub>1</sub>' is the number of accepted dose estimates from synthetic aliquots (i.e. summing of the single-grain data), 'N' is the number of measured single-grains, 'n<sub>2</sub>' is the number of accepted dose estimates from single-grain data, 'n<sub>w.b.</sub>' is the number of grains identified to be well-bleached by the IEU minimum dose model using the given dispersion value *a* (see text for details), 'IEU D<sub>b</sub>' is the burial dose estimated using the IEU and 'Age' is the age derived using the IEU D<sub>b</sub> and the appropriate dose rate (see Table 1).

Fig.1

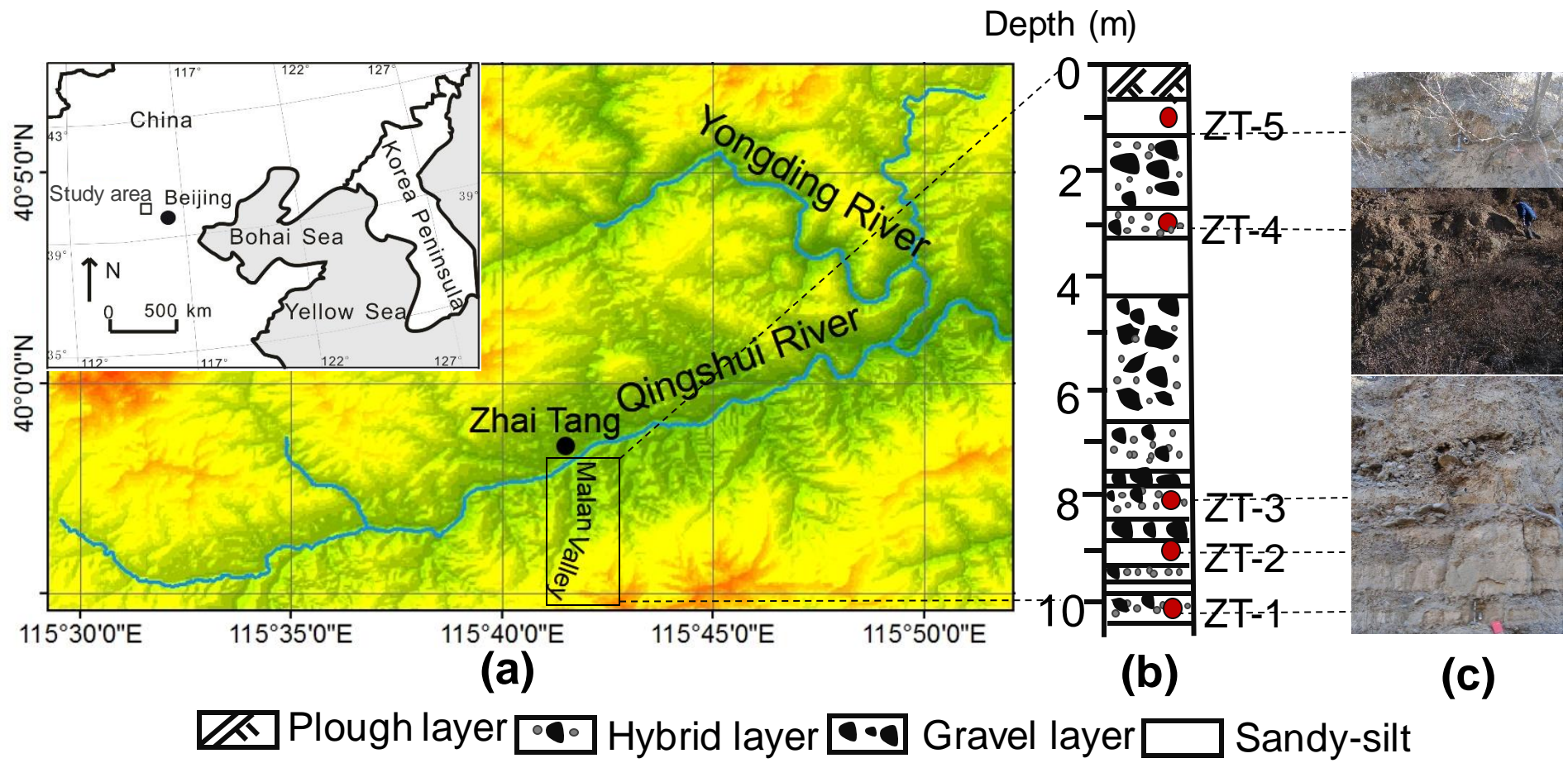


Fig.2

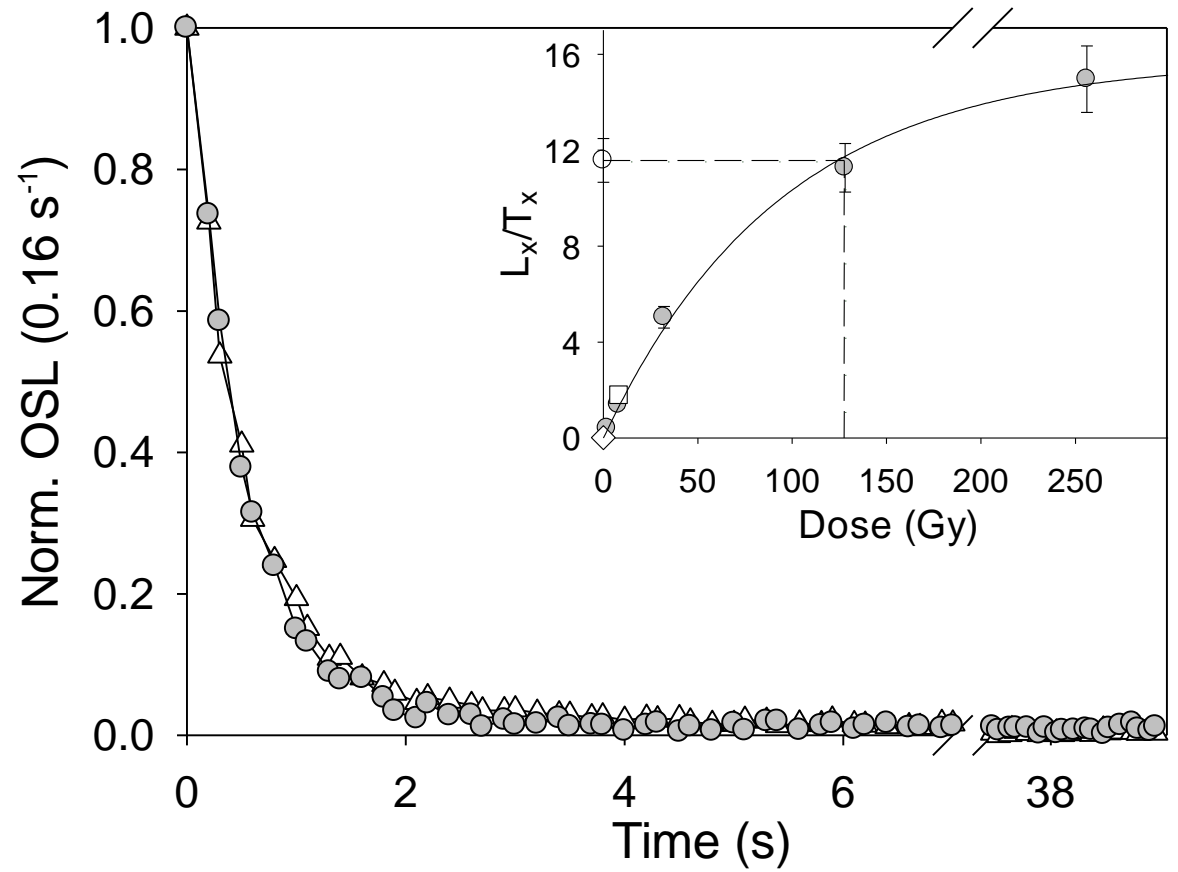


Fig.3

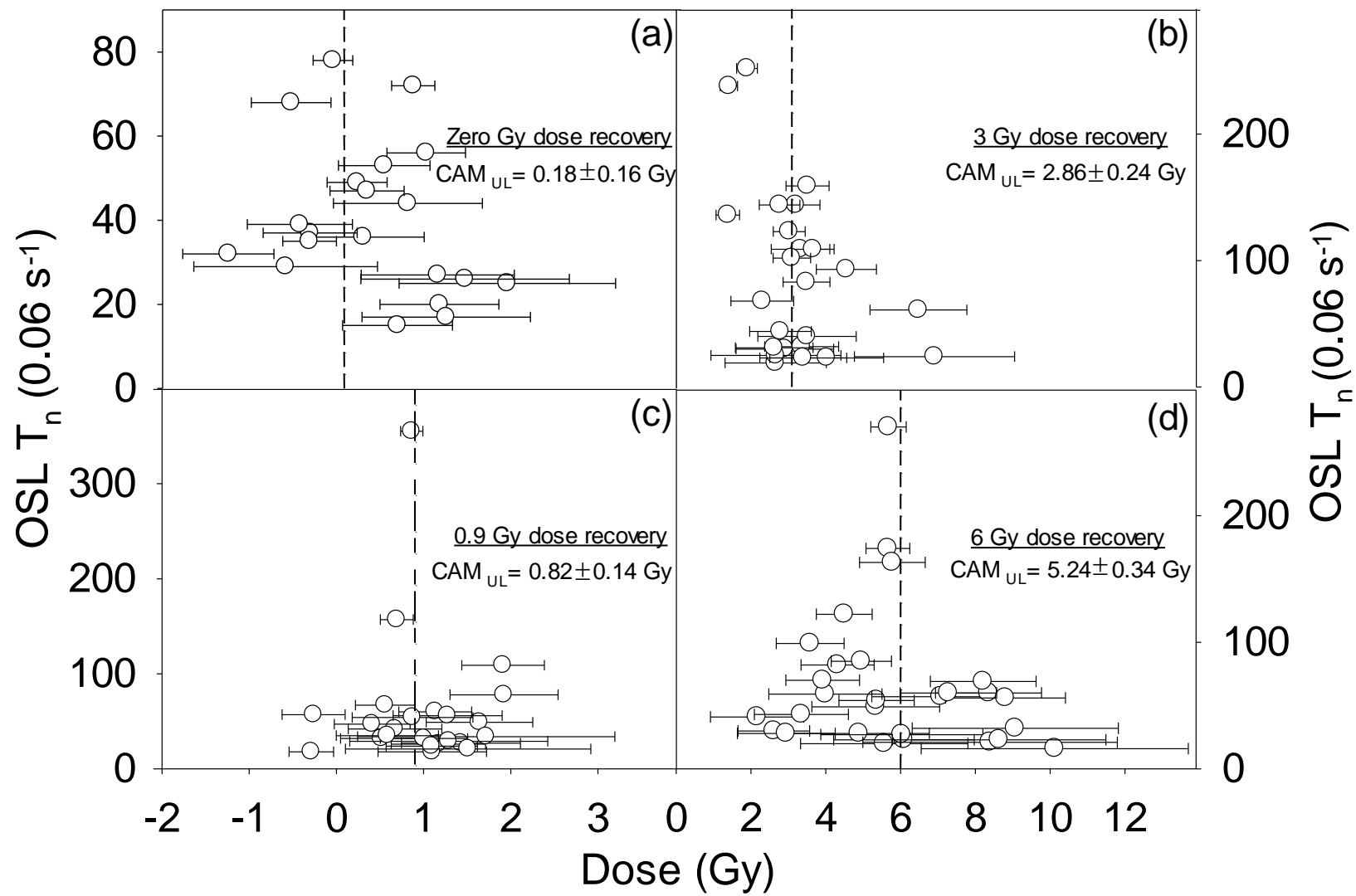


Fig.4

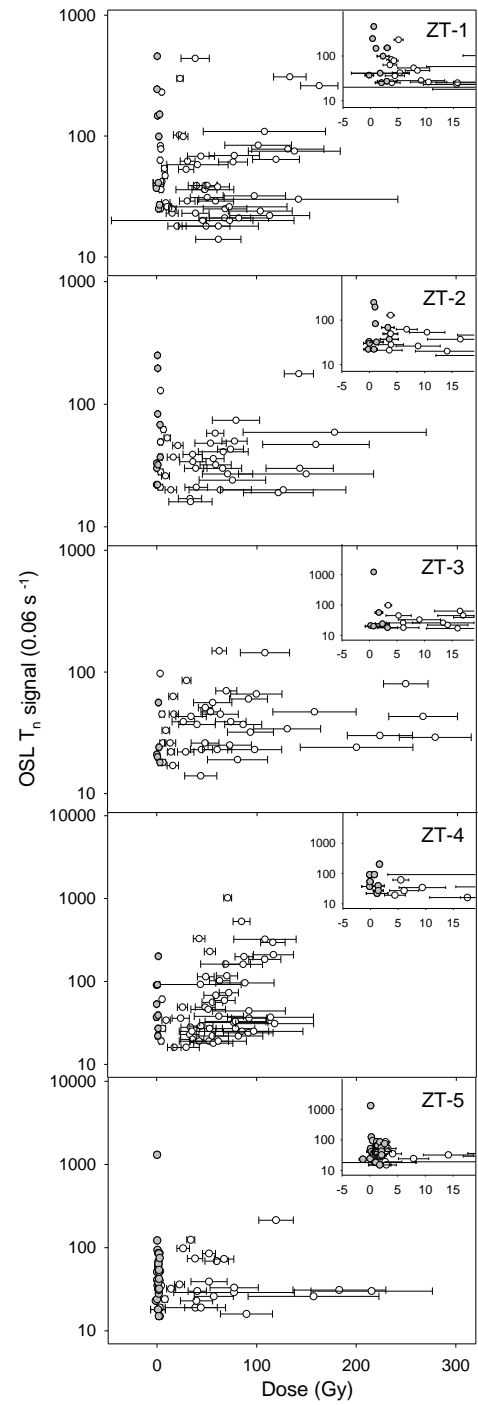


Fig.5

